

Spin-exchange-induced exotic superfluids in a Bose-Fermi spinor mixture

Chuanzhou Zhu¹, Li Chen², Hui Hu³, Xia-Ji Liu³, and Han Pu¹

¹*Department of Physics and Astronomy, and Rice Center for Quantum Materials,
Rice University, Houston, Texas 77251-1892, USA*

²*Institute of Theoretical Physics and Department of Physics,
State Key Laboratory of Quantum Optics and Quantum Optics Devices,*

and Collaborative Innovation Center of Extreme Optics, Shanxi University, Taiyuan 030006, China

³*Centre for Quantum and Optical Science, Swinburne University of Technology, Melbourne 3122, Australia*

We consider a mixture of spin-1/2 bosons and fermions, where only the bosons are subjected to the spin-orbit coupling induced by Raman beams. The fermions, although not directly coupled to the Raman lasers, acquire an effective spin-orbit coupling through the spin-exchange interaction between the two species. Our calculation shows that this is a promising way of obtaining spin-orbit coupled Fermi gas without Raman-induced heating, where the long-sought topological Fermi superfluids and topological bands can be realized. Conversely, we find that the presence of fermions not only provides a new way to create the supersolid stripe phase of the bosons, but more strikingly it can also greatly increase the spatial period of the bosonic density stripes, and hence makes this phase directly observable in experiment. This system provides a new and practical platform to explore the physics of spin-orbit coupling.

Introduction — In recent years, spin-orbit (SO) coupling in cold atoms [1–4] has received tremendous attention. Experimental realization of SO coupled bosons [5–9] and fermions [10–15] has been reported around the world. The interest in such systems is mainly due to the exotic phases induced by SO coupling in quantum gases. For example, SO coupled Bose-Einstein condensates (BEC) can host a stripe phase featuring spatially modulated density profiles [16–22], which can be regarded as a supersolid [9]; whereas SO coupled attractive Fermi gas can become a topological superfluid, supporting Majorana edge states [23–34]. However, the spatial period of the stripe phase is on the order of the optical wavelength, making its direct observation extremely challenging, although indirect evidences for the stripe phase have been reported in two seminal experiments [8, 9]. Another serious experimental problem for realizing SO coupling in quantum gas concerns the heating due to the Raman beams. The Raman-induced heating is particularly severe for atomic species with small fine-structure splitting [35]. Wei and Mueller carefully analyzed the heating problems for all alkali-metal atoms [35]. According to their analysis, ⁴⁰K and ⁶Li — the two most commonly used fermionic species in cold atom experiments — suffer greatly from such heating. This could explain why an SO coupled fermionic superfluid, despite its tremendous theoretical interest, has yet to be realized in experiment.

Here we consider a mixture of bosonic and fermionic superfluids, each of which is a spin-1/2 system. In addition to the density-density interactions, there exists an inter-species spin-exchange interaction. We assume that the condensate is subjected to the Raman-induced SO coupling, whereas the Fermi gas is not coupled by the Raman beams and hence is immune from the Raman-induced heating. The key observation of this Letter is that, through the spin-exchange interaction, the

Fermi gas experiences a significant effective SO coupling. The interplay between the bosons and fermions leads to a variety of interesting quantum states, including a stripe phase in condensate with the spatial period much larger than the optical wavelength, and various topological phases for fermions. Note that a Bose-Bose spinor mixture has been realized in a recent experiment, and the associated effects of spin-exchange interaction were observed [36] and theoretically analyzed [37]. In addition, several groups have created Bose-Fermi superfluid mixtures with scalar condensates [38–41].

Hamiltonian — The total Hamiltonian of the system takes the form (we take $\hbar = 1$)

$$\mathbf{H} = \int dx \left(\Psi_B^\dagger h_B \Psi_B + \Psi_F^\dagger h_F \Psi_F \right) + \mathcal{G}_B + \mathcal{G}_F + \mathcal{G}_{BF}, \quad (1)$$

where $\Psi_B(x) = [\psi_{B\uparrow}(x), \psi_{B\downarrow}(x)]^T$ represents the mean-field wave function of the BEC, and $\Psi_F(x) = [\psi_{F\uparrow}(x), \psi_{F\downarrow}(x)]^T$ denotes the field operator of the Fermi gas. Both species have two internal spin states, which are labelled as \uparrow and \downarrow . The single-particle Hamiltonians h_B and h_F are given by

$$h_B = \frac{(k - k_r \sigma_B^z)^2}{2m_B} + \frac{\Omega_B}{2} \sigma_B^x + \frac{\delta_B}{2} \sigma_B^z, \quad (2)$$

$$h_F = \frac{(k - k_r \sigma_F^z)^2}{2m_F} + \frac{\delta_F}{2} \sigma_F^z, \quad (3)$$

with Ω_B the Raman coupling strength, k_r the Raman recoil momentum, and $\sigma_{B,F}^x$ and $\sigma_{B,F}^z$ the Pauli matrices. We set the two-photon detuning $\delta_B = \delta_F = 0$ in our discussion. For simplicity, we assume that the system is one dimensional. The qualitative physics is insensitive to the dimensionality.

The last three terms in Eq. (1) describe three types of two-body interactions, where the Bose-Bose interactions

read as

$$\mathcal{G}_B = \int dx [g^B (\rho_{B\uparrow}^2 + \rho_{B\downarrow}^2) + 2g_{\uparrow\downarrow}^B \rho_{B\uparrow} \rho_{B\downarrow}], \quad (4)$$

with $\rho_{B\sigma} = |\psi_{B\sigma}(x)|^2$ the spin- σ density of the BEC, the Fermi-Fermi interaction takes the form

$$\mathcal{G}_F = g^F \int dx \psi_{F\uparrow}^\dagger \psi_{F\uparrow}^\dagger \psi_{F\downarrow} \psi_{F\downarrow}, \quad (5)$$

and the Bose-Fermi interactions are given by

$$\mathcal{G}_{BF} = \int dx [\gamma \rho_B \hat{\rho}_F + \beta (\psi_{B\downarrow}^* \psi_{B\uparrow} \psi_{F\uparrow}^\dagger \psi_{F\downarrow} + h.c.)], \quad (6)$$

where $\rho_B = \rho_{B\uparrow} + \rho_{B\downarrow}$ is the density of bosons, and $\hat{\rho}_F = \psi_{F\uparrow}^\dagger \psi_{F\uparrow} + \psi_{F\downarrow}^\dagger \psi_{F\downarrow}$ is the density operator for fermions. Here we have assumed that the inter-species density-density interactions are spin-independent, with a single interaction strength γ , to avoid the proliferation of parameters. The last term in Eq. (6) describes the inter-species spin-exchange interaction characterized by the strength β .

We will consider a one dimensional system with spatial width L with periodic boundary condition. The number of bosons and fermions are given by $N_{B,F}$, with the corresponding average densities $n_{B,F} = N_{B,F}/L$.

Non-interacting fermions — Let us first consider the case with non-interacting fermions, i.e., $g^F = 0$. Previous studies of SO coupled BEC have shown that, in the absence of the fermions, the mean-field wave function of the condensate Ψ_B can be accurately described by the following ansatz:

$$\frac{\Psi_B}{\sqrt{n_B}} = \left[C_1 \begin{pmatrix} \cos \theta \\ -\sin \theta \end{pmatrix} e^{ik_B x} + C_2 \begin{pmatrix} \sin \theta \\ -\cos \theta \end{pmatrix} e^{-ik_B x} \right], \quad (7)$$

where k_B , θ , C_1 and C_2 are variational parameters. We can restrict $k_B \geq 0$ and $\theta \in [0, \pi]$ without loss of generality, and restrict C_1 and C_2 to be real positive numbers, with normalization condition $C_1^2 + C_2^2 = 1$, as the relative phase between them will not affect the total energy. Based on the values of the parameters, three phases of the SO coupled BEC can be identified: the stripe phase (ST) with $B \equiv C_1 C_2 \neq 0$ and $k_B \neq 0$ where the condensate density profile shows the stripe pattern; the plane-wave phase (PW) with $B = 0$ and $k_B \neq 0$ where the BEC condenses into a plane-wave state with finite spin polarization; and the zero-momentum phase (ZM) with $B = 0$ and $k_B = 0$ where the BEC features a smooth density profile with zero spin polarization. Given the variational ansatz (7), the BEC energy functional $\mathbf{E}_B(k_B, \theta, B)$, corresponding to $\int dx \Psi_B^* h_B \Psi_B + \mathcal{G}_B$, is given by

$$\frac{\mathbf{E}_B(k_B, \theta, B)}{N_B} = \frac{k_B^2 + k_r^2 - 2k_r k_B \cos(2\theta)}{2m_B} - \frac{\Omega_B}{2} \sin(2\theta) - F(B) \cos^2(2\theta) + G_1 (1 + 2B^2), \quad (8)$$

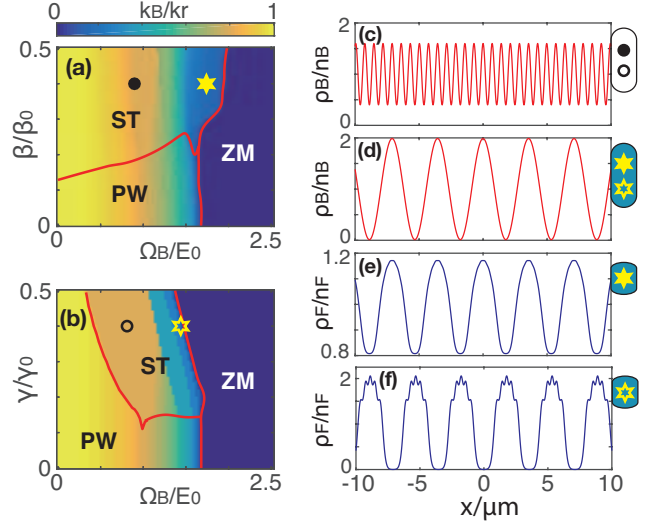


FIG. 1. Phase diagrams of the BEC characterizing the stripe (ST), plane-wave (PW), and zero-momentum (ZM) phases in (a) Ω_B - β plane with $\gamma = 0$, and (b) Ω_B - γ plane with $\beta = 0$, in the case of Fermi-Fermi interaction $g^F = 0$ and the density of bosons $n_B = 10n_F$, where the background color displays the value of k_B/k_r . The Bose condensate density profiles (c) for the black dot and black circle, and (d) for the yellow solid star and yellow hollow star, in the ST phases of the two phase diagrams. The density profiles of the Fermi gas are plotted in (e) and (f) for the yellow solid star in (a) and the yellow hollow star in (b), respectively. The corresponding marks are shown at the right hand side of each density profile. The fermion number is set as $N_F = 2000$. The mass ratio is taken to be $m_B/m_F = 4$. We define the Fermi momentum $k_F = \pi n_F/2$ where $n_F = N_F/L$ is the total fermion density, and $\beta_0 = \gamma_0 = E_0/k_F$ where $E_0 = k_F^2/(2m_F)$. The Raman recoil momentum is taken to be $k_r = 5k_F/4$. The condensate interaction strengths are taken to be $g^B = 6.48 \times 10^{-3} k_r/(2m_B)$ and $g_{\uparrow\downarrow}^B = 2g^B$. In (c)(d)(e)(f), we set $k_r = \sqrt{2\pi}/(804.1\text{nm})$ [7] to convert the length unit to μm .

where we have defined $F(B) = (2G_1 + 4G_2)B^2 - G_2$ and $G_{1,2} = n_B (g^B \pm g_{\uparrow\downarrow}^B)/2$.

The interplay between the condensate and the fermions is reflected in the \mathcal{G}_{BF} term in Eq. (6). We include its effect in an effective fermionic single-particle Hamiltonian h_F^{eff} defined as

$$\int dx \Psi_F^\dagger h_F^{\text{eff}} \Psi_F = \int dx \Psi_F^\dagger h_F \Psi_F + \mathcal{G}_{BF}. \quad (9)$$

Since Eq. (7) is quite general, we assume that the condensate wave function in the presence fermions can still be faithfully represented by Eq. (7). It follows that

$$h_F^{\text{eff}}(k_B, \theta, B) = \frac{(k - k_r \sigma_F^z)^2}{2m_F} + n_B \begin{pmatrix} \gamma V & -\beta M \\ -\beta M^* & \gamma V \end{pmatrix}, \quad (10)$$

where

$$M \equiv \frac{\sin(2\theta)}{2} + B \sin^2 \theta e^{-2ik_B x} + B \cos^2 \theta e^{2ik_B x}; \quad (11)$$

$$V \equiv 2B \sin(2\theta) \cos(2k_B x) + 1. \quad (12)$$

Diagonalizing h_F^{eff} gives a set of fermionic single-particle states. Then the total energy of fermions $\mathbf{E}_F(k_B, \theta, B)$ is obtained by summing up the lowest N_F energies of states under the Fermi sea. The ground state is obtained by minimizing the total energy functional $\mathbf{E}_B(k_B, \theta, B) + \mathbf{E}_F(k_B, \theta, B)$ with respect to the variational parameters (for more details, see the Supplemental Material [42]). In our result, the final values of θ and k_B roughly keep the relation $\cos(2\theta) \approx k_B/k_r$.

This procedure allows us to present the phase diagram of condensate as shown in Fig. 1, where we take $n_B = 10n_F$ and $N_F = 2000$. To isolate the two types of inter-species interactions, we consider in Fig. 1(a) the case with only the spin-exchange interaction ($\gamma = 0$), and in Fig. 1(b) the case with only the density-density interaction ($\beta = 0$).

Figure 1(a) shows the phase diagram of the condensate in the Ω_B - β parameter space. In the absence of fermions, the condensate only possesses two phases, PW and ZM, for $g_{\uparrow\downarrow}^B > g^B$. The transition between them occurs around $\Omega_B = 4k_r^2/(2m_B)$. A notable feature of Fig 1(a) is that the region with large β is dominated by the ST phase. This feature is clearly induced by the fermions. Specifically, the spin-exchange interaction induces an attractive interaction between the two spin components of the condensate, leading to a reduced effective $g_{\uparrow\downarrow}^B$, which favors the ST phase. The background color in Fig. 1(a) displays the value of k_B . In the ST phase, the condensate density profile is given by

$$\rho_B(x) = n_B [1 + \sin(2\theta) \cos(2k_B x)], \quad (13)$$

with a density modulation whose spatial period is determined by $1/k_B$. One can see that, for a given β , k_B decreases as Ω_B increases. Figure 1(c) and (d) show two condensate density profiles corresponding to the black dot and yellow solid star in (a), respectively. For realistic parameters, the ST phase can possess a spatial period of several microns and a large modulation depth. Such a state can be readily observed using *in situ* imaging with today's technology. The density profile for the Fermi gas, corresponding to yellow solid star, is shown in (e). The two density profiles in (d) and (e) exhibit in-phase modulations.

Figure 1(b) represents the condensate phase diagram in the Ω_B - γ parameter space when $\beta = 0$. The qualitative features are similar to that in (a). A large inter-species density-density interaction can also induce the ST phase in condensate, with a controllable k_B as represented by the background color. The bosonic density profiles shown in (c) and (d) also correspond to the black circle and

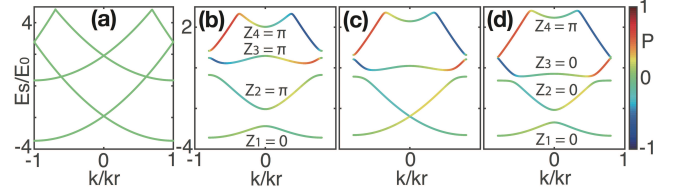


FIG. 2. The lowest four energy bands of the non-interacting fermions with $g^F = 0$, when the condensate is in the ST phase. Here $\beta = 0.6\beta_0$ in all plots. In (a), $\Omega_B = 0$ and $\gamma = 0$. For the rest of the plots, $\Omega_B = E_0$, and $\gamma = 0$ (b), $\gamma = 0.23\gamma_0$ (c), and $\gamma = 0.4\gamma_0$ (d). The Zak phase for each band is indicated in (b) and (d). The color of the curve denotes the spin polarization $P = \langle \sigma_F^z \rangle$. The other parameters are the same as those in Fig. 1.

yellow hollow star in (b), whereas Fig. 1(f) is the Fermi density profile for the yellow hollow star in (b). Here the Bose and Fermi density distributions, as shown in (d) and (f), exhibit out-of-phase modulations. Such a density distribution reduces overlaps between the bosons and fermions, and hence is energetically favored under the repulsive inter-species interaction.

Let us now turn to a more in-depth discussion of the properties of fermions in the mixture. When the condensate is in the PW or the ZM phase, we have $B = 0$, and the effective single-particle Hamiltonian for fermions h_F^{eff} in Eq. (10) is reduced to (after neglecting a term proportional to the constant n_B)

$$h_{F,\text{PW}}^{\text{eff}} = \frac{(k - k_r \sigma_F^z)^2}{2m_F} + \frac{\Omega_F^{\text{eff}}}{2} \sigma_F^x, \quad (14)$$

which has the same form as the Hamiltonian of an SO coupled Fermi gas, only that here the SO coupling is not due directly to the Raman lasers, but to the inter-species spin-exchange interaction with an effective Raman coupling strength given by

$$\Omega_F^{\text{eff}} = -\beta n_B \sin(2\theta). \quad (15)$$

When the condensate is in the ST phase, we have $B = 1/2$, both V and M in Eq. (10) exhibit spatial modulations, originated from the density modulation of the condensate. The V -term, arising from the inter-species density-density interaction, serves as a lattice potential for the fermions, while the M -term, from the spin-exchange interaction, can be regarded as a periodic Raman coupling for the two spin components of the fermions. This situation is analogous to the optical Raman lattice proposed by Liu *et al.* [30, 43], and realized in recent experiments [23, 44]. In the Raman lattice setup, the atom experiences an optical lattice potential and a periodic Raman coupling, both originated from the same laser beams. It is shown that the system parameters can be adjusted and induce topological phase transitions. Drawing from this analogy, we also expect topological

phases in our system. Figure 2 displays the lowest four energy bands E_s of the effective fermionic single-particle Hamiltonian h_F^{eff} in Eq. (10), when the condensate is in the ST phase. In all the plots in Fig. 2, we fix the value of β . Figure 2(a) is a reference plot where $\Omega_B = 0$, hence there is no SO coupling in the system. Here different bands cross each other. The remaining three plots correspond to the same finite value of Ω_B , with varying γ . In these cases, gaps open up at band crossing points in (a). The color of each band represents the spin polarization $P = \langle \sigma_F^z \rangle$, which can be seen to be momentum-dependent — a manifestation of the SO coupling. The values of Z_j , indicated in (b) and (d), are the Zak phase for each band, defined as [45]

$$e^{iZ_j} = \prod_{a=-d}^d w_j^*(k_a) \cdot w_j(k_{a+1}), \quad (16)$$

where $w_j(k_a)$ is the eigenstate of band j and discretized momentum k_a , restricted in the first Brillouin zone in the range $k_a \in [-k_B, k_B]$, with the additional constraint $w_j(k_{d+1}) = w_j(k_{-d})$ to form a loop in the calculation of the Zak phase. At a critical value of γ shown in Fig. 2(c), the lowest two bands crosses each other. When the band reopens at a larger value of γ , the Zak phase of some of the bands changes its value. Thus the closing and the reopening of the band gap signals a topological transition. Note that Zak phase in topological Bloch bands has been measured in recent cold atom experiments [46].

Interacting fermions — Now let us turn to the situation where the fermions are self-interacting with an attractive s -wave interaction strength $g^F = -6k_F/(\pi m_F)$ in Eq. (5), which can lead to superfluid pairing. Including Fermi-Fermi interaction greatly complicates the physics in the ST phase [47]. To keep things relatively simple, we take a large boson density $n_B = 500n_F$, such that in the parameter space we will explore, the bosons are nearly unaffected by the fermions and remain in either the PW or the ZM phase. Under this situation, the effective fermionic single-particle Hamiltonian is given by $h_{F,\text{PW}}^{\text{eff}}$ in Eq. (14). We thus have a system of attractive Fermi gas subjected to SO coupling with an effective Raman coupling strength Ω_F^{eff} defined in Eq. (15). The corresponding fermionic system has been studied before [28] and is known to support topological superfluid phase. This can be intuitively understood as follows. The SO coupling mixes spin singlet and triplet pairings. The Raman term, which can be regarded as an effective Zeeman field, tends to weaken the singlet pairing. For sufficiently large Ω_F^{eff} , the singlet pairing is suppressed, and the Fermi gas becomes a topological superfluid with effective p -wave pairing.

Our calculations indeed confirm this picture [42]. Figure 3(a1) represents the zero temperature phase diagram of the Fermi gas in the Ω_B - β space. It shows three phases: the nontopological superfluid (SF), the topologi-

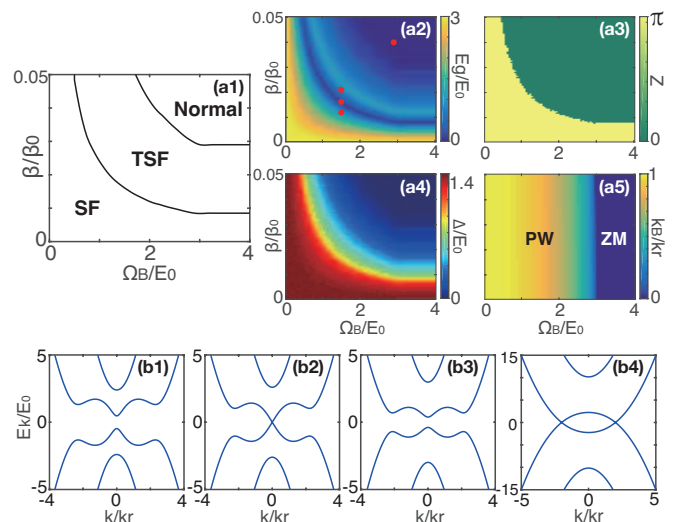


FIG. 3. (a1) The phase diagram of the fermions identifying the superfluid (SF), topological superfluid (TSF), and normal phases in the Ω_B - β parameter space with attractive Fermi-Fermi interaction strength $g^F = -6k_F/(\pi m_F)$ and $n_B = 500n_F$. In the same parameter space, we also plot: (a2) the quasi-particle excitation gap E_g ; (a3) the winding number Z ; (a4) the Fermi superfluid order parameter Δ ; and (a5) the variational momentum k_B of the condensate. The four excitation spectra E_k corresponding to the 4 red dots in (a2), from bottom to top, are plotted in (b1) - (b4), respectively. We take $N_F = 800$. The other parameters are the same as those in Fig. 1.

cal superfluid (TSF), and the normal phases. The former two phases feature finite superfluid order parameter Δ , whereas Δ vanishes in the normal phase, as shown in Fig. 3(a4). The quasi-particle excitation gap E_g is finite in the SF and the TSP phases, except at the boundary of these two, as shown in Fig. 3(a2). Several examples of the quasi-particle excitation spectra E_k at various phases are displayed in Fig. 3(b1)~(b4). The topological phase transition can be further confirmed by the winding number Z , which is defined through a loop connecting the two positive excitation spectra at infinitely large k [42]. As shown in Fig. 3(a3), Z jumps from π to 0 when entering from SF to TSF. Finally, through combining the result of k_B in Fig. 3(a5), the definition of Ω_F^{eff} in Eq. (15), and the relation $\cos(2\theta) = k_B/k_r$, we can see that the TSF phase does correspond to the larger Ω_F^{eff} , and hence our result agrees with our previous picture.

Summary — In summary, we have investigated a system of Bose-Fermi spinor mixtures. The bosons form a condensate that subjected to the Raman-induced SO coupling, while the fermions are not coupled to the Raman lasers, but interact with the bosons via the density-density and/or spin-exchange interaction. We show that the spin-exchange interaction makes the fermions experiencing an effective SO coupling, without suffering Raman-induced heating. This could pave a new way to-

wards the first realization of SO coupled fermionic superfluids, which can be made to be topological with a proper choice of parameters. The interplay between the bosons and fermions also has an interesting effect on the former: the Bose-Fermi interaction (both the density-density and the spin-exchange interactions) favors the condensate to be in the ST phase, with an interaction-dependent spatial modulation period. With realistic parameters, the spatial modulation period can be as large as several microns, making the ST phase readily observable with the *in situ* imaging technique. This provides a significant advantage in both the realization and the observation of the ST phase.

Our proposal does not require any new techniques beyond those that have already been demonstrated in the lab. In particular, both the Bose-Bose spinor mixtures [36] and the Bose-Fermi superfluid mixtures [38–41] have been realized. The density-density interaction strengths have been routinely tuned via Feshbach resonance [48, 49]. Recent works have also shown that the spin-exchange interaction can be tuned to some extent [50–53]. We therefore expect that our proposal will inspire more works, both theoretical and experimental, on SO coupled quantum gas spinor mixture, providing a new and unique platform to explore the physics of SO coupling.

We acknowledge discussions with Xiong-Jun Liu, Randall G. Hulet, and Peng Zhang, and supports from the US NSF and the Welch Foundation (Grant No. C-1669), the NSF of China (Grant No. 11804205), and the Australian Research Council (Grant No. DP170104008).

[1] V. Galitski and I. B. Spielman, *Nature (London)* **494**, 49 (2013).
[2] N. Goldman, G. Juzeliūnas, P. Öhberg, and I. B. Spielman, *Rep. Prog. Phys.* **77**, 126401 (2014).
[3] H. Zhai, *Rep. Prog. Phys.* **78**, 026001 (2015).
[4] W. Zhang, W. Yi, and Carlos A. R. Sá Melo (Eds.) *Synthetic Spin-Orbit Coupling in Cold Atoms*, (World Scientific, 2018).
[5] Y.-J. Lin, R. L. Compton, K. Jiménez-García, W. D. Phillips, J. V. Porto, and I. B. Spielman, *Nat. Phys.* **7**, 531 (2011).
[6] J.-Y. Zhang, S.-C. Ji, Z. Chen, L. Zhang, Z.-D. Du, B. Yan, G.-S. Pan, B. Zhao, Y.-J. Deng, H. Zhai, S. Chen, and J.-W. Pan, *Phys. Rev. Lett.* **109**, 115301 (2012).
[7] Y.-J. Lin, K. Jiménez-García, and I. B. Spielman, *Nature* **471**, 83 (2011).
[8] S.-C. Ji, J.-Y. Zhang, L. Zhang, Z.-D. Du, W. Zheng, Y.-J. Deng, H. Zhai, S. Chen, and J.-W. Pan, *Nat. Phys.* **10**, 314 (2014).
[9] J.-R. Li, J. Lee, W. Huang, S. Burchesky, B. Shteynas, F. Çağrı Top, A. O. Jamison, and W. Ketterle, *Nature* **543**, 91 (2017).
[10] Z. Fu, L. Huang, Z. Meng, P. Wang, L. Zhang, S. Zhang, H. Zhai, P. Zhang, and J. Zhang, *Nat. Phys.* **10**, 110

(2014).

[11] L. W. Cheuk, A. T. Sommer, Z. Hadzibabic, T. Yefsah, W. S. Bakr, and M. W. Zwierlein, *Phys. Rev. Lett.* **109**, 095302 (2012).
[12] P. Wang, Z.-Q. Yu, Z. Fu, J. Miao, L. Huang, S. Chai, H. Zhai, and J. Zhang, *Phys. Rev. Lett.* **109**, 095301 (2012).
[13] M. Lee, J. H. Han, J. H. Kang, M.-S. Kim, and Y. Shin, *Phys. Rev. A* **95**, 043627 (2017).
[14] S. L. Bromley, S. Kolkowitz, T. Bothwell, D. Kedar, A. Safavi-Naini, M. L. Wall, C. Salomon, A. M. Rey, J. Ye, *Nat. Phys.* **14**, 399 (2018).
[15] N. Q. Burdick, Y. Tang, and B. L. Lev, *Phys. Rev. X* **6**, 031022 (2016).
[16] C. Wang, C. Gao, C.-M. Jian, and H. Zhai, *Phys. Rev. Lett.* **105**, 160403 (2010).
[17] T.-L. Ho and S. Zhang, *Phys. Rev. Lett.* **107**, 150403 (2011).
[18] Y. Li, L. P. Pitaevskii, and S. Stringari, *Phys. Rev. Lett.* **108**, 225301 (2012).
[19] Y. Li, G. I. Martone, L. P. Pitaevskii, and S. Stringari, *Phys. Rev. Lett.* **110**, 235302 (2013).
[20] C. Zhu, L. Dong, and H. Pu, *J. Phys. B: At. Mol. Opt. Phys.* **49**, 145301 (2016).
[21] R. Sakamoto, Y. Ono, E. Arahata, and H. Mori, *J. Phys. Soc. Jpn.* **85**, 064401 (2016).
[22] R. Sakamoto, Y. Ono, R. Hatsuda, K. Shiina, E. Arahata, and H. Mori, *J. Phys. Soc. Jpn.* **86**, 075003 (2017).
[23] B. Song, L. Zhang, C. He, T. F. J. Poon, E. Hajiyev, S. Zhang, X.-J. Liu, and G.-B. Jo, *Sci. Adv.* **4**, eaao4748 (2018).
[24] G. Jotzu, M. Messer, R. Desbuquois, M. Lebrat, T. Uehlinger, D. Greif, and T. Esslinger, *Nature (London)* **515**, 237 (2014).
[25] Z. Meng, L. Huang, P. Peng, D. Li, L. Chen, Y. Xu, C. Zhang, P. Wang, and J. Zhang, *Phys. Rev. Lett.* **117**, 235304 (2016).
[26] M. Gong, S. Tewari, and C. Zhang, *Phys. Rev. Lett.* **107**, 195303 (2011).
[27] K. Sun, Z. Gu, H. Katsura, and S. D. Sarma, *Phys. Rev. Lett.* **106**, 236803 (2011).
[28] X.-J. Liu and H. Hu, *Phys. Rev. A* **88**, 023622 (2013).
[29] X.-J. Liu, *Phys. Rev. A* **86**, 033613 (2012).
[30] X.-J. Liu, Z.-X. Liu, and M. Cheng, *Phys. Rev. Lett.* **110**, 076401 (2013).
[31] Y. Oreg, G. Refael, and F. v. Oppen, *Phys. Rev. Lett.* **105**, 177002 (2010).
[32] X.-J. Liu, *Phys. Rev. A* **87**, 013622 (2013).
[33] R. Wei and E. J. Mueller, *Phys. Rev. A* **86**, 063604 (2012).
[34] X.-J. Liu and H. Hu, *Phys. Rev. A* **85**, 033622 (2012).
[35] R. Wei and E. J. Mueller, *Phys. Rev. A* **87**, 042514 (2013).
[36] X. Li, B. Zhu, X. He, F. Wang, M. Guo, Z.-F. Xu, S. Zhang, and D. Wang, *Phys. Rev. Lett.* **114**, 255301 (2015).
[37] L. Chen, C. Zhu, Y. Zhang, and H. Pu, *Phys. Rev. A* **97**, 031601(R) (2018).
[38] I. Ferrier-Barbut, M. Delehaye, S. Laurent, A. T. Grier, M. Pierce, B. S. Rem, F. Chevy, and C. Salomon, *Science* **345**, 1035 (2014).
[39] R. Roy, A. Green, R. Bowler, and S. Gupta, *Phys. Rev. Lett.* **118**, 055301 (2017).
[40] X.-C. Yao, H.-Z. Chen, Y.-P. Wu, X.-P. Liu, X.-Q. Wang, X. Jiang, Y. Deng, Y.-A. Chen, and J.-W. Pan, *Phys.*

Rev. Lett. **117**, 145301 (2016).

[41] J. M. McNamara, T. Jeltes, A. S. Tychkov, W. Hogervorst, and W. Vassen, Phys. Rev. Lett. **97**, 080404 (2006).

[42] See Supplemental Material for more information on the calculation of the ground-state energy of non-interacting fermions, and the mean-field theory for topological phase transition with strong Fermi-Fermi interaction.

[43] X.-J. Liu, K. T. Law, and T. K. Ng, Phys. Rev. Lett. **113**, 059901 (2014).

[44] Z. Wu, L. Zhang, W. Sun, X.-T. Xu, B.-Z. Wang, S.-C. Ji, Y. Deng, S. Chen, X.-J. Liu, and J.-W. Pan, Science **354**, 83 (2016).

[45] J. Zak, Phys. Rev. Lett. **62**, 2747 (1989).

[46] M. Atala, M. Aidelsburger, J. T. Barreiro, D. Abanin, T. Kitagawa, E. Demler, and I. Bloch, Nat. Phys. **9**, 795 (2013).

[47] When the condensate is in the ST phase, fermions experiences a band structure as shown in Fig. 2. In the presence Fermi-Fermi interaction, it becomes a quite difficult problem to treat the bosons and fermions self-consistently for such an inhomogeneous system. We plan to address this problem in the future.

[48] S. Inouye, M. R. Andrews, J. Stenger, H.-J. Miesner, D. M. Stamper-Kurn, and W. Ketterle, Nature **392**, 151 (1998).

[49] C. Chin, R. Grimm, P. Julienne, and E. Tiesinga, Rev. Mod. Phys. **82**, 1225 (2010).

[50] L. Rieger, N. D. Oppong, M. Höfer, D. R. Fernandes, I. Bloch, and S. Fölling, Phys. Rev. Lett. **120**, 143601 (2018).

[51] R. Zhang and P. Zhang, Phys. Rev. A **98**, 043627 (2018).

[52] M. A. Norcia, R. J. Lewis-Swan, J. R. K. Cline, B. Zhu, A. M. Rey, J. K. Thompson, Science **361**, 259 (2018).

[53] J.-J. Chen, Z.-F. Xu, and L. You, Phys. Rev. A **98**, 023601 (2018).

Supplemental Material: Spin-exchange-induced exotic superfluids in a Bose-Fermi spinor mixture

Chuanzhou Zhu¹, Li Chen², Hui Hu³, Xia-Ji Liu³, and Han Pu¹

¹*Department of Physics and Astronomy, and Rice Center for Quantum Materials,*

Rice University, Houston, Texas 77251-1892, USA

²*Institute of Theoretical Physics and Department of Physics,*

State Key Laboratory of Quantum Optics and Quantum Optics Devices,

and Collaborative Innovation Center of Extreme Optics, Shanxi University, Taiyuan 030006, China

³*Centre for Quantum and Optical Science, Swinburne University of Technology, Melbourne 3122, Australia*

In this Supplemental Material, we provide more technical details for the calculation we carried out.

I. CALCULATION OF THE ENERGY OF NON-INTERACTING FERMIONS

In this section, we introduce our approach for obtaining the energy bands and the total energy functional of the effective fermionic single-particle Hamiltonian $h_F^{\text{eff}}(k_B, \theta, B)$ in the main text. We study this Hamiltonian in the plane-wave basis $|k_a + 2nk_B, \sigma\rangle$, where $(k_a + 2nk_B)$ is the momentum and $\sigma = \uparrow, \downarrow$ represents the spin. Taking the periodic boundary condition, we restrict $k_B = 2\pi d/L$ and $k_a = 2\pi a/L$ with integers d , a , and n . The variational parameter k_B (or d) is positive and will be determined later through minimization of the total system energy. Due to the periodicity of the Hamiltonian, k_a is restricted in the first Brillouin zone as $k_a \in [-k_B, k_B]$ (or equivalently $a \in [-d, d-1]$). For each k_a in the Brillouin zone, the basis with different values of n and σ span a subspace, in which the Hamiltonian takes the matrix form

$$h_{F,k_a}^{\text{eff}} = \begin{bmatrix} \ddots & \ddots & 0 & 0 & 0 \\ \ddots & D_{k_a}^{n-1} & U^T & 0 & 0 \\ 0 & U & D_{k_a}^n & U^T & 0 \\ 0 & 0 & U & D_{k_a}^{n+1} & \ddots \\ 0 & 0 & 0 & \ddots & \ddots \end{bmatrix}, \quad (1)$$

with the diagonal block $D_{k_a}^n$ given by

$$D_{k_a}^n = \begin{bmatrix} \epsilon_{k_a,\uparrow}^n & \frac{1}{2}\Omega_F^{\text{eff}} \\ \frac{1}{2}\Omega_F^{\text{eff}} & \epsilon_{k_a,\downarrow}^n \end{bmatrix}, \quad (2)$$

where $\epsilon_{k_a,\uparrow}^n = (k_a + 2nk_B \mp k_r)^2 / (2m_F)$ and $\Omega_F^{\text{eff}} = -\beta n_B \sin(2\theta)$ is the effective Raman coupling for the Fermi gas as defined in Eq. (15) in the main text, and with the off-diagonal block U given by

$$U = n_B B \begin{bmatrix} \gamma \sin(2\theta) & -\beta \cos^2 \theta \\ -\beta \sin^2 \theta & \gamma \sin(2\theta) \end{bmatrix}. \quad (3)$$

In the matrix in Eq. (1), we take $n \in [-n_{\text{max}}, n_{\text{max}}]$ with a large cut-off n_{max} such that the momentum

$(k_a + 2n_{\text{max}}k_B)$ is far beyond the Fermi surface. After we numerically diagonalize the Hamiltonian h_{F,k_a}^{eff} for all k_a in the Brillouin zone, we obtain the total energy of fermions $\mathbf{E}_F(k_B, \theta, B)$ by summing up the energies of the lowest N_F states under the Fermi sea. Then the ground-state values of variational parameters are determined by minimizing the total energy functional $\mathbf{E}_B(k_B, \theta, B) + \mathbf{E}_F(k_B, \theta, B)$, where \mathbf{E}_B is the energy contributed by the bosons, as defined in Eq. (8) in the main text.

II. CALCULATION FOR INTERACTING FERMIONS

In this section, we introduce our mean-field calculation for the ground state of the mixture in the case of strong Fermi-Fermi interaction with $g^F = -6k_F / (\pi m_F)$. As we discussed in the main text, we consider the case of $n_B = 500n_F$ and $g_{\uparrow\downarrow}^B = 2g^B$, under which condition, the bosons are restricted in the PW or ZM phase which features a flat density profile. The condensate wavefunction takes the form of Eq. (7) in the main text, just as in the case of non-interacting fermions. Similarly, the bosonic contribution to the total energy functional $\mathbf{E}_B(k_B, \theta, B)$ still takes the form of Eq. (8) in the main text, only that the parameter B vanishes for the PW and the ZM phase.

For the fermion part, the thermodynamic grand potential corresponding to the $\int dx \Psi_F^\dagger h_F \Psi_F + \mathcal{G}_{BF} + \mathcal{G}_F$ term in the whole mixture Hamiltonian is given by

$$\mathbf{P}_F(\mu, \theta) = \int dx \Psi_F^\dagger (h_{F,\text{PW}}^{\text{eff}} - \mu) \Psi_F + \mathcal{G}_F, \quad (4)$$

where μ is the chemical potential, and $h_{F,\text{PW}}^{\text{eff}}$ and \mathcal{G}_F are defined by Eqs. (14) and (5) in the main text, respectively. Note that $h_{F,\text{PW}}^{\text{eff}}$ is a function of the variational parameter θ . In our treatment of the fermionic part, we follow the standard mean-field approach introduced for the single-species interacting fermions as reported in, e.g., Refs [1, 2]. In the mean-field approximation, the Fermi-Fermi interaction term turns to be

$$\mathcal{G}_F = -\Delta \left[\psi_{F\uparrow}^\dagger(x) \psi_{F\downarrow}^\dagger(x) + \text{h.c.} \right] - \Delta^2 / g^F, \quad (5)$$

where the superfluid order parameter is defined as $\Delta = -g^F \langle \psi_{F\downarrow}(x) \psi_{F\uparrow}(x) \rangle$. Through the Fourier transformation $\psi_\sigma(x) = L^{-1/2} \sum_k e^{ikx} c_{k\sigma}$ with the momentum $k = 2\pi a/L$, the integer a taken from $-\infty$ to ∞ in the summation, the system length L , and the spin $\sigma = \uparrow, \downarrow$, the grand potential can be re-written as

$$\mathbf{P}_F(\mu, \theta, \Delta) = \frac{1}{2} \sum_k C_k^\dagger M_k C_k + \sum_k \xi_k - \frac{L\Delta^2}{g^F}, \quad (6)$$

where $C_k^\dagger = [c_{k\uparrow}^\dagger \ c_{k\downarrow}^\dagger \ c_{-k\uparrow}^\dagger \ c_{-k\downarrow}^\dagger]$ and

$$M_k = \begin{bmatrix} \xi_k + \lambda k & \Omega_F^{\text{eff}}/2 & 0 & -\Delta \\ \Omega_F^{\text{eff}}/2 & \xi_k - \lambda k & \Delta & 0 \\ 0 & \Delta & -\xi_k + \lambda k & -\Omega_F^{\text{eff}}/2 \\ -\Delta & 0 & -\Omega_F^{\text{eff}}/2 & -\xi_k - \lambda k \end{bmatrix}, \quad (7)$$

with $\xi_k = k^2/(2m_F) - \mu$ and $\lambda = -k_r/m_F$. Through analytically diagonalizing the matrix M_k , we further transform the grand potential to the form

$$\begin{aligned} \mathbf{P}_F(\mu, \theta, \Delta) &= \frac{1}{2} \sum_k (E_{k1} \alpha_{k1}^\dagger \alpha_{k1} + E_{k2} \alpha_{k2}^\dagger \alpha_{k2} \\ &+ E_{k3} \alpha_{k3}^\dagger \alpha_{k3} + E_{k4} \alpha_{k4}^\dagger \alpha_{k4}) + \sum_k \xi_k - \frac{L\Delta^2}{g^F}, \end{aligned} \quad (8)$$

where α_{k1} , α_{k2} , α_{k3} , and α_{k4} are quasi-particle elementary excitation operators with the symmetry $E_{k4} = -E_{-k1}$ and $E_{k3} = -E_{-k2}$. The two positive excitation spectra are given by

$$E_{k1,2} = \left(\xi_k^2 + \eta_k + \Delta^2 \pm \sqrt{4\eta_k \xi_k^2 + (\Omega_F^{\text{eff}})^2 \Delta^2} \right)^{\frac{1}{2}}, \quad (9)$$

with $\eta_k = (k_r k/m_F)^2 + (\Omega_F^{\text{eff}})^2/4$. The ground state of the fermions is considered to be the quasi-particle vac-

uum, with the corresponding ground-state grand potential given by

$$\mathbf{P}_F(\mu, \theta, \Delta) = -\frac{1}{2} \sum_k (E_{k1} + E_{k2}) + \sum_k \xi_k - \frac{L\Delta^2}{g^F}, \quad (10)$$

where the anti-commutation relations of α_{k1} , α_{k2} , α_{k3} , and α_{k4} have been considered. Note that $\mathbf{P}_F(\mu, \theta, \Delta)$ is a functional of three undetermined variational parameters μ , θ , and Δ .

The ground state of the whole mixture is obtained through the minimization of $\mathbf{E}_B(k_B, \theta, 0) + \mathbf{P}_F(\mu, \theta, \Delta)$ with respect to the variational parameters k_B , θ , and Δ , where the constraint $N_F = -\partial \mathbf{P}_F(\mu, \theta, \Delta)/\partial \mu$ is imposed to fix the number of fermions. Actually, the minimization of $\mathbf{E}_B(k_B, \theta, 0)$ with respect to k_B leads to the rigorous relation $\cos(2\theta) = k_B/k_r$, and hence we only need to deal with θ and Δ in the numerical minimization. The converged results of k_B , θ , Δ , and μ are obtained in the thermodynamic limit with $N_B, N_F, L \rightarrow \infty$ while $n_B = N_B/L$ and $n_F = N_F/L$. In the main text, the results of Δ and k_B are shown in Fig. 3(a4) and (a5), and the resulting spectrum gaps shown in Fig. 3(a2) and the excitation spectra shown in Fig. 3(b1-b4) are obtained by substituting the resulting variational parameters back into Eq. (9). Finally, the winding number Z shown in Fig. 3(a3) is obtained as

$$e^{iZ} = \prod_{a=-b}^b [w_1^*(k_a) \cdot w_1(k_{a+1})] [w_2^*(k_a) \cdot w_2(k_{a+1})], \quad (11)$$

where $w_1(k_a)$ and $w_2(k_a)$ are the quasiparticle eigenstates corresponding to the two positive excitation spectra E_{k1} and E_{k2} in Eq. (9), with the quasi-momentum defined as $k_a = 2\pi a/L$ with the integer $a \in [-b, b]$ with b a sufficiently large numerical cut-off. We define $w_1(k_{b+1}) = w_2(k_{-b})$ and $w_2(k_{b+1}) = w_1(k_{-b})$ to connect the two positive excitation spectra and form the loop in calculating the winding number. Note that here k_a in (11) is no longer restricted in the first Brillouin zone.

[1] X.-J. Liu and H. Hu, Phys. Rev. A **88**, 023622 (2013).
[2] R. Wei and E. J. Mueller, Phys. Rev. A **86**, 063604 (2012).